

## Tuning the performance of pyrido[4,3-b]pyrazine-EDOT hybrid polymers for use as neutral green electrochromic materials

Faqi Hu<sup>1,2</sup>, Qi Zhao<sup>1,2</sup>, Ying Li<sup>3,\*</sup>, Ximei Liu<sup>1,\*</sup>

<sup>1</sup> School of Pharmacy, Jiangxi Science and Technology Normal University, Nanchang 330013, Jiangxi, PR China

<sup>2</sup> Flexible Electronics Innovation Institute (FEII), Jiangxi Science and Technology Normal University, Nanchang 330013, Jiangxi, PR China

<sup>3</sup> Business School, Jiangxi Science and Technology Normal University, Nanchang 330013, Jiangxi, PR China

\*E-mail: [916749930@qq.com](mailto:916749930@qq.com) ; [lxm5812@163.com](mailto:lxm5812@163.com)

*Received:* 8 November 2020 / *Accepted:* 18 December 2020 / *Published:* 31 December 2020

---

Conjugated electrochromic polymers have been reported for many years, owing to their multicolor display, minimal energy consumption, and excellent stability. Among them, there are very few polymers with a neutral green color and desirable performance. In this work, we developed a series of neutral green/gray electrochromic materials by tuning the performance of pyrido[4,3-b]pyrazine-EDOT hybrid polymers. The synthesized precursors/polymers were characterized by optoelectronic, morphological, computational, electrochemical, and electrochromic methods. Results showed that introducing a methyl-substituted pyrido[4,3-b]pyrazine acceptor into the molecular design improved the solubility of the precursors (EPMPE and BEPMPBE) and the redox stability of the corresponding polymers (PEPMPE and PBEPMPBE). On the other hand, the extended conjugated chain redshifted the absorption spectra of the polymers (PBEPPE and PBEPMPBE), which changed their color from neutral green to gray, but also reduced their optical bandgap, and further improved their optical contrast, response time, and even coloration efficiency in the near-infrared region. The excellent electrochromic performance and rare color of the pyrido[4,3-b]pyrazine-EDOT hybrid polymers make them promising materials for use in near-infrared electrochromic applications.

---

**Keywords:** Conjugated polymer, Electrochromism, Pyrido[4,3-b]pyrazine, EDOT, Green color

### 1. INTRODUCTION

Conjugated electrochromic polymers have been reported for 50 years since the 1970s. [1] Generally, among these reports there are criteria that must be met when designing an electrochromic material with satisfactory properties, such as high coloration efficiency, a fast response time, excellent

optical contrast, a low bandgap, and multicolor change. [2, 3] Typically, effective shortcuts to adjust the properties and color of electrochromic polymers usually involve using the D-A strategy, which consists of modifying with substituents and increasing the length or planarity of the conjugated backbone. To date, a series of D-A-D type polymers with advantageous electrochromism has been obtained by either our group or other groups [4-11] and the color display covers almost the entire spectrum based on the three basic colors of RGB; however, neutral green polymers are still relatively rare. [12]

According to the subtractive process of color mixing theory, a polymer that exhibits a neutral green color should contain at least two simultaneous absorption bands in the red and blue regions of the visible spectrum when the same voltage is applied. [4] This stringent requirement makes an electrochromic green polymer rare. In some early reports, pyrido[3,4-b]pyrazine (PP) and its derivatives were demonstrated to be admirable blocks for the synthesis of neutral green and low bandgap-conjugated polymers [13] due to the strong electron affinity of the three imine nitrogens in the PP structure. [13-15] Similar to quinoxaline, [16] PP can also be easily modified by introducing substituents, such as alkyl or alkoxy chains at its 2 and 3 positions, which will affect the solubility of the conjugated polymer and in turn change its optoelectronic, electrochemical, and electrochromic properties. [17, 18]

On the other hand, 3,4-ethylenedioxythiophene (EDOT) has proven to be one of the most commonly used donors for the construction of low bandgap compounds, which is attributed to its strong electron-donating property, good planarity, and easy modifiability of its active sites. [5, 7, 19, 20] In contrast, as a derivative of EDOT, bis(2-(3,4-ethylenedioxy)thienyl) (BisEDOT) has a lower HOMO-LUMO gap and stronger electron-donating ability. [6, 21] In addition, the longer conjugate structure of BisEDOT activates the hydrogen atom at the  $\alpha$ -position on the thiophene ring, which is beneficial when designing molecules with lower polymerization potential. [22, 23]

Based on the above considerations, in this work, we designed and synthesized BisEDOT, 5,8-dibromopyrido[3,4-b]pyrazine, and 5,8-dibromo-2,3-dimethylpyrido[3,4-b]pyrazine as building blocks for the rational construction of novel green electrochromic polymers. Four precursors (EPPE, EPMPE, BEPPBE, and BEPMPBE) were synthesized through a *Stille* coupling reaction employing PP or pyrido[3,4-b]methylpyrazine (PMP) as acceptors and EDOT or BisEDOT as donors. The corresponding polymers were synthesized by electropolymerization (Scheme 1), and their structure-property relationships in regard to optoelectronics, morphology, electrochemistry, and electrochromism were systematically studied.

## 2. EXPERIMENTAL

### 2.1 Chemicals

Synthetic materials, such as 2,5-dibromopyridine-3,4-diamine (98%; Shanghai Vita Chemical), glyoxal (98%; Shanghai Vita Chemical), 2,3-butanedione (98%; Energy Chemical), 3,4-ethylenedioxythiophene (EDOT, 98%; Energy Chemical), *n*-butyllithium (*n*-BuLi, 1.6 M hexanes;

J&K Chemical), chlorotributyltin ( $\text{SnBu}_3\text{Cl}$ , 98%; Energy Chemical), and anhydrous ethanol (EtOH, analytical grade; Shanghai Vita Chemical), were purchased from guaranteed chemical plants and used without further purification for the synthesis of precursors. Tetrahydrofuran (THF, analytical grade; Xilong Chemical) was used as a solvent for the monostannylation of EDOT, dimethylformamide (DMF, analytical grade; Xilong Chemical) was used as a solvent for *Stille* coupling, and dichloromethane ( $\text{CH}_2\text{Cl}_2$ , analytical grade; Energy Chemical) was used for precursor purification and electrochemical experiments, which were purified by distillation with sodium in a nitrogen atmosphere before use. Tetrabutylammonium hexafluorophosphate ( $\text{Bu}_4\text{NPF}_6$ , 99%; Energy Chemical) was dried under vacuum at  $100^\circ\text{C}$  for 12 h as the electrolyte for the electrochemical experiments. Tetrakis(triphenylphosphine)palladium (0) ( $\text{Pd}(\text{PPh}_3)_4$ , 99%; J&K) and copper chloride ( $\text{CuCl}_2$ , 99%; Sigma-Aldrich) were used as the catalyst for *Stille* coupling and the synthesis of BisEDOT, respectively. Other chemicals and reagents were analytical grade and used without any further treatment.

## 2.2 Molecules Synthesis

The synthetic route and condition of the precursors and intermediates are depicted in Scheme 1. 2,3-Dihydro-5-(2,3-dihydrothieno[3,4-b][1,4]dioxin-5-yl)thieno[3,4-b][1,4]dioxine (BisEDOT), 2-tributylstannyl-3,4-ethylenedioxythiophene (monostannylation of EDOT), and 2-tributylstannyl-2,3-dihydro-5-(2,3-dihydrothieno[3,4-b][1,4]dioxin-5-yl)thieno[3,4-b][1,4]dioxine (monostannylation of BisEDOT) were synthesized according to our previous works. [5, 6]

5,8-dibromopyrido[3,4-b]pyrazine (Br-PP-Br): 2,5-Dibromopyridine-3,4-diamine (5.03 g, 18.70 mmol) and glyoxal (3.42 g, 56.2 mmol) were added to anhydrous EtOH (200 mL) and stirred at  $70^\circ\text{C}$  for 12 h in a nitrogen atmosphere. Then, the mixture was cooled to room temperature and transferred to an aqueous ice solution. The organic phase was separated with  $\text{CH}_2\text{Cl}_2$  and then dried over anhydrous  $\text{Mg}_2\text{SO}_4$  before purification by silica column chromatography. The obtained product was a yellow solid with a yield of 85%.  $^1\text{H}$  NMR (400 MHz,  $\text{CDCl}_3$ )  $\delta$  9.11 (s, 1H), 9.04 (s, 1H), 8.77 (s, 1H) (Fig. S1 in the Supplementary Material).

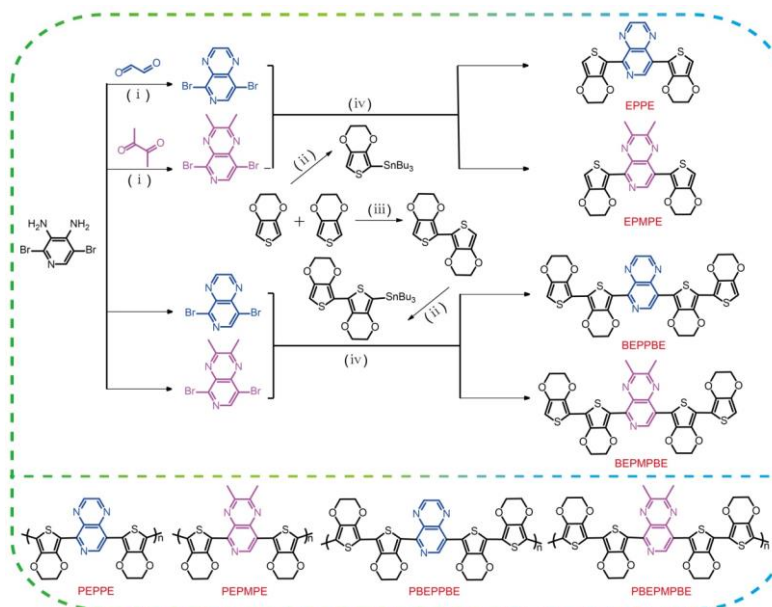
5,8-dibromo-2,3-dimethylpyrido[3,4-b]pyrazine (Br-PMP-Br): 2,5-Dibromopyridine-3,4-diamine (4.05 g, 15.18 mmol) and 2,3-butanedione (2.61 g, 30.36 mmol) were added to anhydrous EtOH (120 mL) and stirred at  $70^\circ\text{C}$  for 12 h in a nitrogen atmosphere, and then similar purification steps as those used for Br-PP-Br were performed. The obtained product was a yellow solid with a yield of 90%.  $^1\text{H}$  NMR (400 MHz,  $\text{CDCl}_3$ )  $\delta$  8.63 (s, 1H), 2.80 (s, 6H). (Fig. S2).

5,8-Bis(2,3-dihydrothieno[3,4-b][1,4]dioxin-5-yl)pyrido[3,4-b]pyrazine (EPPE):  $\text{Pd}(\text{PPh}_3)_4$  (0.50 g, 0.52 mmol) was added to a deoxidized solution of 5,8-dibromopyrido[3,4-b]pyrazine (1.57 g, 5.20 mmol) and unpurified 2-tributylstannyl-3,4-ethylenedioxythiophene (15.42 g, 41.53 mmol) in dry DMF (50 mL). The mixture was heated to  $100^\circ\text{C}$  and refluxed for an additional 12 h in a nitrogen atmosphere, and then excess solvent was removed by rotary evaporation and extracted with  $\text{CH}_2\text{Cl}_2$  in saturated aqueous brine. The organic phase was separated and washed twice with water and then dried over anhydrous  $\text{Mg}_2\text{SO}_4$  before purification by silica column chromatography ( $\text{CH}_2\text{Cl}_2$ :petroleum ether

(PE), 1:1). The obtained EPPE was a yellow solid with a yield of 71%.  $^1\text{H}$  NMR (400 MHz,  $\text{DMSO-}d_6$ )  $\delta$  9.51 (s, 1H), 9.12 (s, 2H), 6.90 (d,  $J = 25.7$  Hz, 2H), 4.43-4.30 (m, 8H) (Fig. S3).

5,8-bis(2,3-dihydrothieno[3,4-b][1,4]dioxin-5-yl)-2,3-dimethylpyrido[3,4-b]pyrazine (EPMPE):  $\text{Pd}(\text{PPh}_3)_4$  (0.36 g, 0.31 mmol) was added to a deoxidized solution of 5,8-dibromo-2,3-dimethylpyrido[3,4-b]pyrazine (1.03 g, 3.15 mmol) and unpurified 2-tributylstannyl-3,4-ethylenedioxythiophene (6.82 g, 18.90 mmol) in dry DMF (30 mL). After that, the reaction conditions of the mixture and the treatment of the crude product were the same as those of EPPE to obtain EPMPE as a yellow solid with a yield of 80%.  $^1\text{H}$  NMR (400 MHz,  $\text{CDCl}_3$ )  $\delta$  9.70 (s, 1H), 6.65 (s, 1H), 6.57 (s, 1H), 4.48 (d,  $J = 7.9$  Hz, 2H), 4.35 (d,  $J = 18.7$  Hz, 6H), 2.82 (d,  $J = 5.0$  Hz, 6H) (Fig. S4).

5,8-bis(2,2',3,3'-tetrahydro-[5,5'-bithieno[3,4-b][1,4]dioxin]-7-yl)pyrido[3,4-b]pyrazine (BEPPE):  $\text{Pd}(\text{PPh}_3)_4$  (0.1 g, 0.11 mmol) was added to a deoxidized solution of 5,8-dibromopyrido[3,4-b]pyrazine (0.30 g, 1.046 mmol) and unpurified 2,3-dihydro-5-(2,3-dihydrothieno[3,4-b][1,4]dioxin-5-yl)thieno[3,4-b][1,4]dioxine (2.99 g, 5.228 mmol) in dry DMF (20 mL). After that, the reaction conditions of the mixture and the treatment of the crude product were the same as those of EPPE to obtain BEPPE as a dark purple solid with a yield of 65%.  $^1\text{H}$  NMR (400 MHz,  $\text{DMSO-}d_6$ )  $\delta$  9.53 (s, 1H), 9.16 (d,  $J = 33.8$  Hz, 2H), 6.66 (d,  $J = 16.3$  Hz, 2H), 4.53-4.27 (m, 16H) (Fig. S5).



**Scheme 1** Synthetic routes of the four precursors and their corresponding polymers. Reagents and conditions: (i) EtOH, 70°C, 12 h; (ii) *n*-BuLi, THF, -78°C, 4 h, then  $\text{SnBu}_3\text{Cl}$ , -40°C, 6 h; (iii) *n*-BuLi, THF, -78°C, 1 h, then  $\text{CuCl}_2$ , 0°C, 12 h; and (iv)  $\text{Pd}(\text{PPh}_3)_4$ , refluxing DMF, 12 h.

2,3-dimethyl-5,8-bis(2,2',3,3'-tetrahydro-[5,5'-bithieno[3,4-b][1,4]dioxin]-7-yl)pyrido[3,4-b]pyrazine (BEPMPBE):  $\text{Pd}(\text{PPh}_3)_4$  (0.2 g, 0.46 mmol) was added to a deoxidized solution of 5,8-dibromo-2,3-dimethylpyrido[3,4-b]pyrazine (1.48 g, 4.68 mmol) and unpurified 2,3-dihydro-5-(2,3-dihydrothieno[3,4-b][1,4]dioxin-5-yl)thieno[3,4-b][1,4]dioxine (10.86 g, 29.86 mmol) in dry DMF (40

mL). After that, the reaction conditions of the mixture and the treatment of the crude product were the same as those of EPPE to obtain BEPMPBE as a dark purple solid with a yield of 54%.  $^1\text{H}$  NMR (400 MHz,  $\text{DMSO-}d_6$ )  $\delta$  9.35 (s, 1H), 6.54 (d,  $J = 14.0$  Hz, 2H), 4.30 (dd,  $J = 42.3, 37.9$  Hz, 16H), 2.82-2.68 (m, 6H) (Fig. S6).

### 2.3 Instrumentation and characterization

The NMR spectra of the precursors and typical intermediates were recorded for structural identification with an NMR spectrometer (Bruker AV 400, Germany). Optical characterization of the UV-vis absorption spectra and fluorescence emission spectra for precursors were performed on an ultraviolet-visible spectrophotometer (SPECORD 200 PLUS, Germany) and fluorescence spectrophotometer (F-4600, Hitachi, Japan), respectively. Infrared spectra were obtained using a Fourier transform infrared (FT-IR) spectrometer (Bruker Vertex 70, Germany) with the samples pressed into KBr pellets. Theoretical calculations of the four precursors were studied by density functional theory (DFT) with the Gaussian 03 program package. The surface morphology of polymer films deposited onto the surface of ITO glass in a doped or dedoped state were investigated by scanning electron microscopy (acceleration voltage of 5.0 kV; SU8220, Hitachi, Japan).

### 2.4 Electropolymerization and electrochemical tests

By potentiostatic polymerization, polymers (PEPPE, PEPMPPE, PBEPMPBE, and PBEPPE) were obtained for further optical, morphological, electrochemical, and electrochromic characterization, and the structures are shown in Scheme 1. All electropolymerization and electrochemical tests were performed using a three-electrode system in a one-compartment electrolytic cell by a Versa Stat 3 electrochemical workstation (EG&G Princeton Applied Research). Electrochemical tests were mainly aimed at exploring the oxidation activity of the precursors and the electrochemical stability of the polymers. The treatment details of the electrode used and the deoxygenation of the electrolyte solution were consistent with our previous reports. [5, 11]

### 2.5 Spectroelectrochemical and kinetic studies

Spectroelectrochemical and kinetic studies were performed by combining a UV-vis spectrophotometer (SPECORD 200, Germany) and an electrochemical workstation (Versa Stat 3, EG&G Princeton Applied Research) using a three-electrode system with a transparent cuvette. Specific details are available in our previous report. [5] For the spectroelectrochemical test, the UV-vis absorption spectra of polymer films at varying potentials were obtained to evaluate the optical and color changes. In regard to the kinetic studies, the time-transmittance profiles were recorded for the further calculation of the optical contrast, response time, coloration efficiency, and open-circuit memory properties of the polymers.

### 3. RESULTS AND DISCUSSION

#### 3.1 Molecular design

Based on the admirable acceptor PP and the powerful donor EDOT, we also introduced methyl groups and another EDOT to modify PP and EDOT, respectively, thereby obtaining the acceptor PMP and the donor BisEDOT. Through the *Stille* coupling reaction, four neutral green/gray electrochromic molecules (EPPE, EPMPE, BEPPBE, and BEPMPBE) were designed and synthesized, and the corresponding polymers were also polymerized electrochemically. These four polymers not only provided a chance to understand the effect of a substituent on the electrochemical and electrochromic performance of a D-A-D system but also provided an opportunity to observe the modulation of the color display by extended conjugated chains in the molecule.

#### 3.2 Optical property

To understand the relationship between the optical properties and structures of different precursors, the absorption and emission spectra of the four precursors were examined in CH<sub>2</sub>Cl<sub>2</sub>, as illustrated in Fig. 1, and the related optical parameters are summarized in Table 1. The UV-vis absorption spectra (Fig. 1A) show a banded double-peak shape, which is consistent with the characteristics of D-A-D-type compounds. [11, 24, 25] The absorption peaks in the high-energy band region (300-400 nm) were attributed to the  $\pi$ - $\pi^*$  electronic transition of the conjugated system, [5] while the absorption peaks in the long-wavelength region (400-600 nm) could be caused by charge transfer between the donor and acceptor. [26, 27]

Comparing the absorption spectrum of EPMPE with that of EPPE or the absorption spectrum of BEPMPBE with that of BEPPBE, it can be observed that the absorption peaks of EPMPE and BEPMPBE blueshift due to the substitution effect of the methyl groups. Moreover, the absorption peaks of EPMPE or BEPMPBE have no significant shift in the high-energy band region, while a larger shift appears in the low-energy band region. This result may reflect that the substituent effect has a greater impact on the charge transfer between donor and acceptor. [7] On the other hand, as the donors change, the absorption peaks of BEPPBE and BEPMPBE redshift in contrast with that of EPPE and EPMPE. This result may be ascribed to the regulation of the extended conjugated chain on the molecular bandgap. In addition, since the absorption peaks in the visible light region change significantly, the color of the corresponding polymer is modulated. [3, 9]

From the fluorescence emission spectra (Fig. 1B), all the emission peaks of the four precursors are in the range of 604-742 nm (Table 1). Similar to the exhibited rule of the UV-vis absorption spectra, the emission spectra also shift to the high-energy band region from EPPE to EPMPE (approximately 30 nm) and from BEPPBE to BEPMPBE (approximately 50 nm). As the electron-donating capability of the donor increases, a redshift in the emission peaks of BEPPBE and BEPMPBE is also observed relative to that of EPPE and EPMPE.

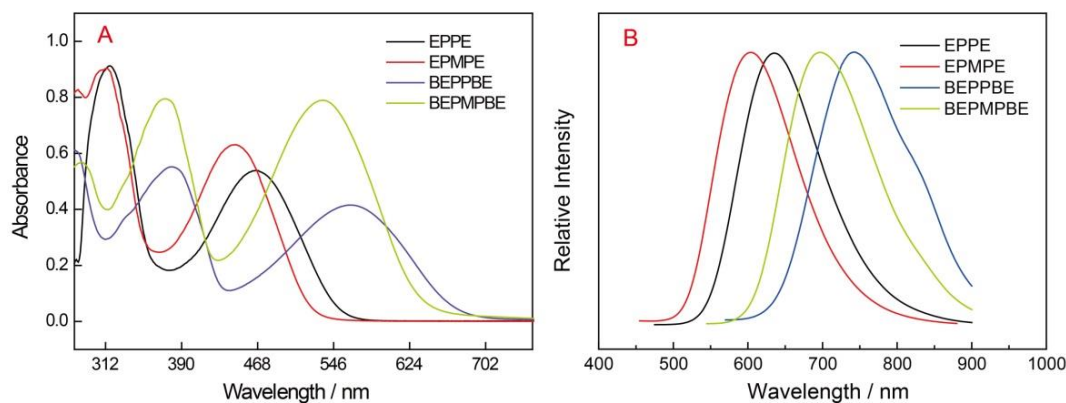


**Figure 1.** UV-vis absorption (A) and fluorescence emission (B) spectra of the four precursors in  $\text{CH}_2\text{Cl}_2$ .

**Table 1.** Optical, electrochemical and calculated parameters of the four precursors

Precursors	$\lambda_{\text{max},1}$ (nm)	$\lambda_{\text{max},2}$ (nm)	$\lambda_{\text{em}}$ (nm)	$E_{\text{ox,onset}}$ (V)	$E_{\text{HOMO,DFT}}$ (eV)	$E_{\text{LUMO,DFT}}$ (eV)	HOMO-LUMO gap (eV)	Dihedral angles (deg)	HOMO	LUMO
EPPE	317	466	637	0.88	-5.82	-1.60	4.22	37.53, 8.56 (PP-EDOT)		
EPMPE	313	444	604	0.82	-5.73	-1.37	4.36	-3.35, 38.27 (PMP-EDOT)		
BEPPBE	382	562	742	0.72	-5.82	-1.58	4.24	35.40, 7.75 (PP-BisEDOT) -1.24, -2.75 (EDOT-EDOT)		
BEPMPBE	373	535	697	0.71	-5.09	-1.39	3.70	37.38, 12.87 (PMP-BisEDOT) 1.38, -3.10 (EDOT-EDOT)		

### 3.3 Electrochemical polymerization of the four precursors

The electropolymerization behavior and conditions of the four precursors were examined in a  $\text{CH}_2\text{Cl}_2\text{-Bu}_4\text{NPF}_6$  ( $0.10 \text{ mol L}^{-1}$ ) system. In Fig. 2A-2D, the oxidation onset potential decreases from 0.88 V (EPPE) to 0.82 V (EPMPE), and from 0.72 V (BEPPBE) to 0.71 V (BEPMPBE). From these results, it can be concluded that introducing alkyl groups into the molecular design has advantages in lowering the oxidation onset potential of these molecules. With the appearance of stronger donors, BisEDOT elongates the  $\pi$ -conjugated chain and further modulates the electronic nature of the

molecules, which makes BEPPBE and BEPMPBE more easily oxidized than EPPE and EPMPE. [28, 29]

Cyclic voltammograms of the four precursors (Fig. 2E-2H) were recorded to observe their potentiodynamic electropolymerization behavior. Along with the increase in the number of scanning cycles, the current densities in the CVs increase evenly, which indicates that the amount of conductive polymer also uniformly increases on the working electrode. [11, 30] Furthermore, as the anode peak shifts positively and the cathode peaks shift negatively, an additional potential is used to overcome the resistance of the increased polymer content. [19] The redox peaks of the four polymers in the CVs are distributed with broad waves, which suggest that the deposited polymer chains have a wide length distribution.[5, 19]. Notably, the oxidation peak current density of the four precursors increase in the order of EPPE<EPMPE<BEPPBE<BEPMPBE. This phenomenon reflects that grafting an alkyl chain on the acceptor and combining the acceptor with a strong donor can be beneficial to the formation of high-quality films. [7, 8]

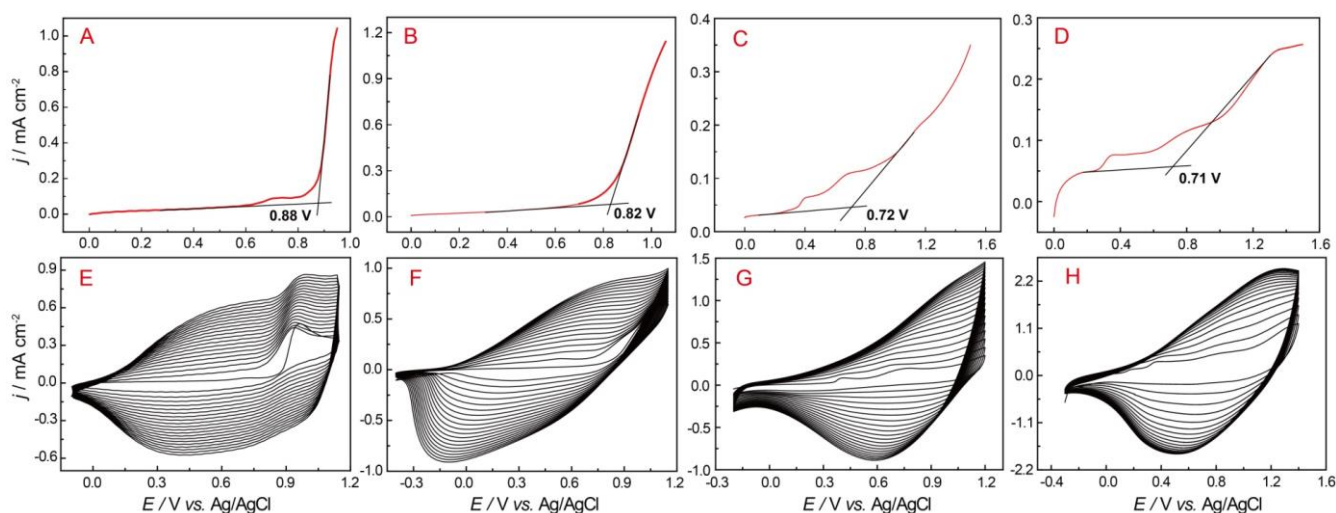


**Figure 2** Anodic oxidation curves and cyclic voltammograms (CVs) of 0.05 mol L<sup>-1</sup> EPPE (A, E), EPMPE (B, F), BEPPBE (C, G), and BEPMPBE (D, H) on a Pt working electrode in CH<sub>2</sub>Cl<sub>2</sub>-Bu<sub>4</sub>NPF<sub>6</sub> (0.10 mol L<sup>-1</sup>). Potential scan rate: 50 mV s<sup>-1</sup>; Scanning cycles: 20.

### 3.4 Structural characterization

It has been reported that the electropolymerization position of EDOT end-capped precursors will only appear on the C<sub>α</sub> of thiophene rings according to the radical cation mechanism. [25, 31] To expound on this structure and verify the electropolymerization position of EPPE, EPMPE, BEPPBE, and BEPMPBE, the FT-IR spectra of the precursors and corresponding polymers are depicted in Fig. 3, and detailed absorption peak assignments are summarized in Table S1-S2 in the Supplementary Material.

From the black curves in Fig. 3, the peaks of the four precursors at approximately 3101-2871 cm<sup>-1</sup>, 1207-1061 cm<sup>-1</sup>, and 911-801 cm<sup>-1</sup> are attributed to the =C-H stretching vibration and in-plane and out-of-plane bending vibrations of the thiophene rings, respectively. These peaks all disappear or

are weakened in the spectra of the corresponding polymers (red curves in Fig. 3). This phenomenon is consistent with previous reports, which further explains why the four precursors are electropolymerized by coupling at the C<sub>α</sub> positions of EDOT. [5, 11, 32] In the spectra of the polymers, the absorption peaks of the pyridine and thiophene rings do not significantly disappear, indicating that the structure of the components is not damaged after polymerization. [19] In addition, owing to the poor uniformity of the chain length of the newly obtained polymers, the vibration peaks at different positions overlap together, and a broad absorption peak appears in the infrared absorption spectra of the polymers.

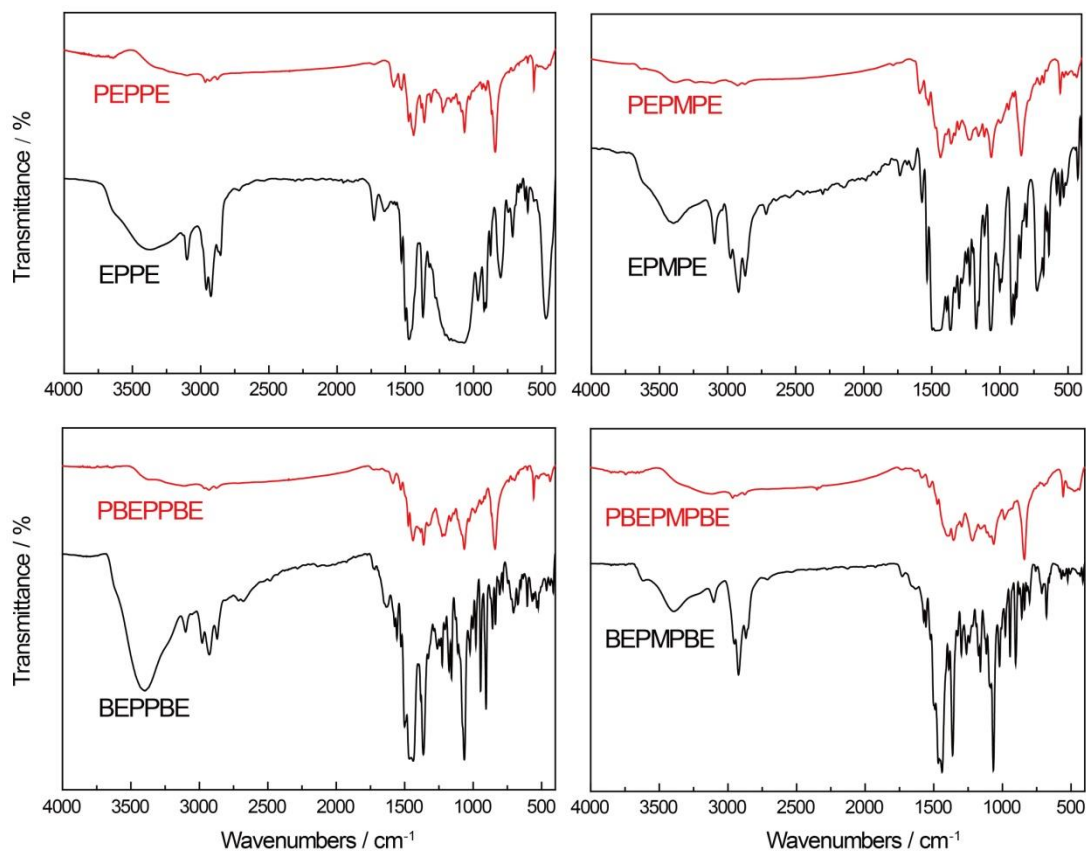


**Figure 3.** Fourier transform infrared (FT-IR) spectra of the four precursors and corresponding polymers.

### 3.5 Computational results and Morphology

The results of computation by density functional theory (DFT) are useful to evaluate the electronic structure of multielectron conjugated precursors and polymers. [33] At the B3LYP/6-31G level, the optimized dihedral angles, HOMO/LUMO values, energy level distribution diagrams, and corresponding HOMO-LUMO gaps are summarized in Table 1, and the optimized geometries under different views are shown in Table S3. From the optimal geometries and dihedral angles of the precursors, it can be seen that all the precursors show relatively planar structures (close to 0°), which can contribute to a higher degree of  $\pi$ -electron coupling and further lower the HOMO-LUMO gap.

[34] According to frontier orbital theory, atoms in a molecule with a higher HOMO proportion are more likely to provide electrons to generate radical cations for easier electropolymerization. [19, 35] Clearly, the HOMO proportion at the  $\alpha$ -positions of the thiophene ring in EDOT is much higher than that of other atoms from the HOMO orbital distribution, and together with the stronger steric hindrance effect at the  $\beta$ -positions in the thiophene ring, it can be reasonably deduced that electropolymerization should preferentially occur at the  $\alpha$ -positions of the thiophene ring in EDOT. [11, 35]

The surface morphology of the PEPPE, PEPMPE, PBEPPBE, and PBEPMPBE films is recorded in Fig. 4, which is helpful to realize the redox activity and stability of the polymers. The SEM images of PEPPE and PEPMPE in the dedoped state present fine particle and rod-like morphologies, and these morphologies do not change significantly after doping, implying the stability of the polymers. In addition, from the SEM images of PBEPPBE and PBEPMPBE, the deposited particle size is larger and denser after the increase in the conjugated chain length. Notably, the surface of doped PBEPMPBE is porous, which makes the migration of ions in the structure easier during the redox process and may improve the optical contrast and conversion time of the material. [19]

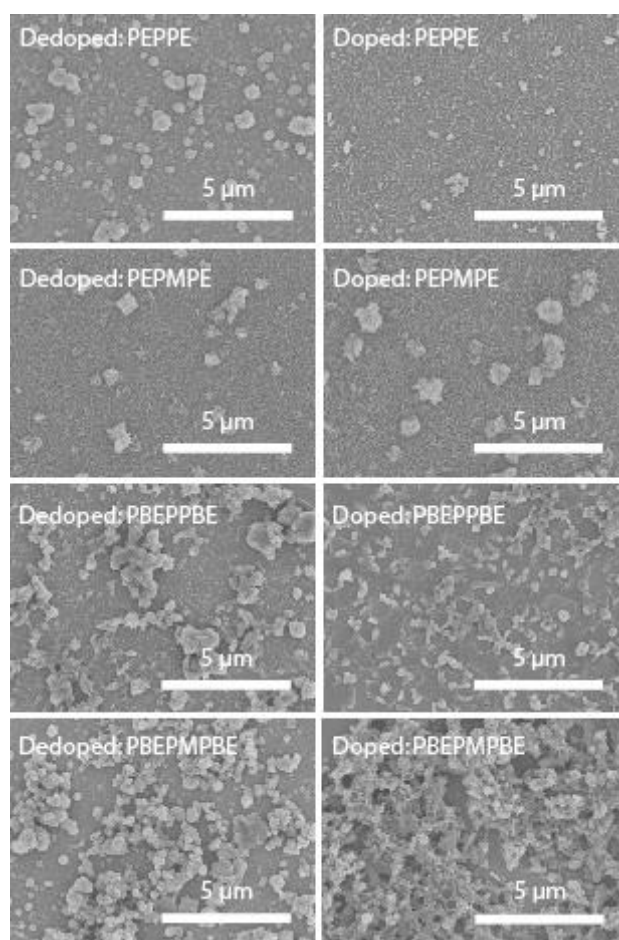


**Figure 4.** Scanning electron microscopy (SEM) images of the PEPPE, PEPMPE, PBEPPBE, and PBEPMPBE films through dedoping/doping at -0.2 V/1.3 V, 0.2 V/1.4 V, -0.2 V/1.3 V, and -0.3 V/1.2 V, respectively. Acceleration voltage: 5.0 kV, Magnification: 10000 $\times$ .

## 3.6 Electrochemistry of polymers

The CVs of the polymers were obtained to gain new insights into the electrochemical properties of polymers, especially in terms of their electrochemical activity and stability. [10, 36] In Fig. 5A-5D, the CVs of the four polymers recorded in a blank electrolyte solution of  $\text{CH}_2\text{Cl}_2$  exhibit broad redox peaks, which is characteristic of EDOT-based polymers and in good agreement with the CVs of the precursors. [6, 24, 25] Similar broad peaks also exist in the CVs measured in the MeCN solution (Fig. S7), implying that the solvent has no significant effect on the electrochemical behavior of the four polymers. Notably, the CVs of the PEPMPE and PBEPMPBE films have sharper redox peaks than those of the PEPPE and PBEPPE films, indicating the faster doping/dedoping rate of the PEPMPE and PBEPMPBE films. This phenomenon may be attributed to the larger steric hindrance caused by methyl substitution, which makes the polymer chain more dispersed, thus facilitating the free passage of the counter ions of the dopant in the conjugate block. [34] Moreover, all the anodic and cathodic peak current densities in the CV of each polymer are proportional to the scanning speed, as shown in Fig. 5E-5H, implying that the deposited conductive materials are well attached to the electrode and do not exhibit obvious diffusion. [8, 11]

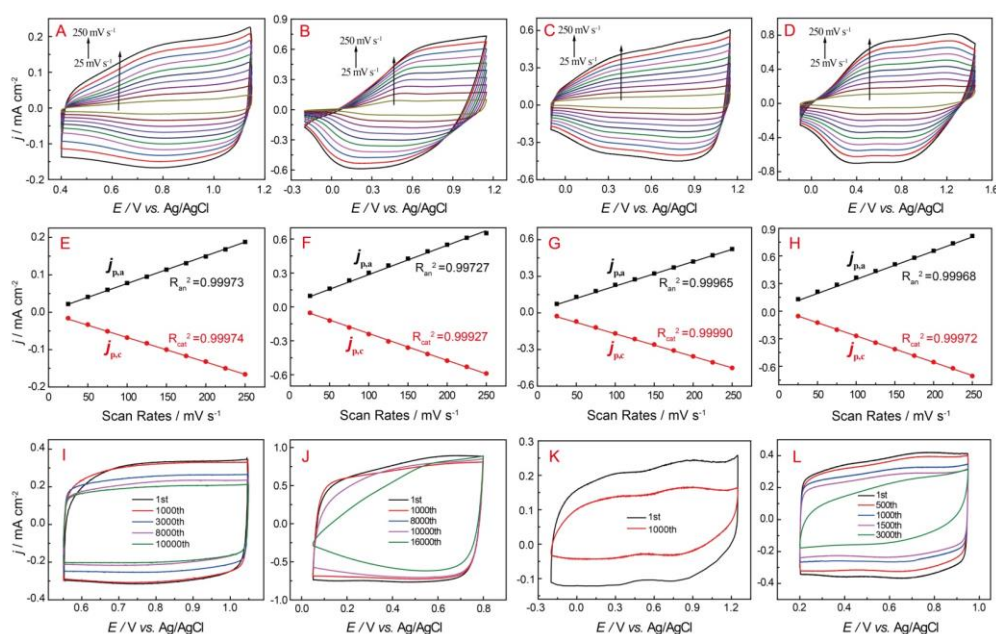


**Figure 5.** Top: CVs of the PEPPE (A), PEPMPE (B), PBEPPE (C), and PBEPMPBE (D) films in blank  $\text{CH}_2\text{Cl}_2\text{-Bu}_4\text{NPF}_6$  ( $0.10 \text{ mol L}^{-1}$ ) at potential scan rates of 250, 200, 150, 100, 50, and  $25 \text{ mV s}^{-1}$ . Middle: Plots of the redox peak current densities versus potential scan rates of the PEPPE (E), PEPMPE (F), PBEPPE (G), and PBEPMPBE (H) films,  $j_{p,a}$  and  $j_{p,c}$  denote the anodic and cathodic peak current densities, respectively. Bottom: Long-term CVs of PEPPE (I), PEPMPE (J), PBEPPE (K), and PBEPMPBE (L) in blank  $\text{MeCN-Bu}_4\text{NPF}_6$  ( $0.10 \text{ mol L}^{-1}$ ) at a potential scan rate of  $150 \text{ mV s}^{-1}$ . The polymer films were deposited electrochemically on a Pt electrode at optimal potentials for 30 s.

It is known that stability in reversible redox processes is critical for the application of polymers in electronic devices. The long-term CVs in Fig. 5I-5L were obtained in a blank MeCN solution to examine the stability of the four polymers, and the parameters are recorded in Table 2. The electrical activity of PEPPE and PEPMPE after 10000 cycles is maintained at 66% and 89%, respectively, and for PEPMPE, it stays above 71% after 16000 cycles, making them promising materials for use in electronic devices. The stability of PBEPPE and PBEPMPBE is inferior to that of PEPPE and PEPMPE, and only 51% and 76% of their electrical activity remains after 1000 scanning cycles, which probably accounts for their decrease in electroactivity. This decrease is due to the dissolution and diffusion of oligomers intermingled in the polymers, and the degradation of conductive substances on the main chain by the organic solvent. [19, 34]

**Table 2.** Electrochemical and spectroelectrochemical parameters of the green color polymers

Polymers	Electrochemistry		Redox stability		Spectroelectrochemistry		Color conversion	
	$E_{\text{ox,peak}}$ (V)	$E_{\text{red,peak}}$ (V)	1000 <sup>th</sup>	10000 <sup>th</sup>	$\lambda_{\text{onset}}$ (nm)	$E_{\text{g,opt}}$ (eV)	Reduction	Oxidation
PEPPE	0.85	0.80	99%	66%	1227	1.01		
PEPMPE	0.70	0.15	94%	89%	1150	1.08		
PBEPPE	0.87	0.77	52%	–	875	1.42		
PBEPMPBE	1.20	0.32	76%	44% (3000 <sup>th</sup> )	1510	0.82		
PBOTT-BTD <sup>[37]</sup>	-	-	-	-	-	1.51	green	blue
PIDOHE <sup>[7]</sup>	0.05	-0.66	-	-	-	1.27	green	gray
PIDODE <sup>[7]</sup>	0	-0.64	-	-	-	1.26	green	gray
PEPTE <sup>[34]</sup>	-	-	-	-	-	1.12	green	blue

### 3.7 Electrochromic properties

#### 3.7.1 Spectroelectrochemistry

Spectroelectrochemistry is an effective method to observe the optical absorption and color conversion of polymers. Therefore, the optical absorption spectra at different voltage pulses were recorded to monitor the electrochromic behaviors of the four polymers electrodeposited on ITO-coated glass. In Fig. 6A-6D, as the applied voltage increases, the doping degree of the polymers gradually increases. The absorption spectra of the polymer films redshift, and the polymers undergo a color transition, as shown in Table 2. Specifically, the absorption peaks in the visible region gradually decrease until new absorption peaks appear in the near-infrared region, which corresponds to the transformation of the charge carrier in the conjugated structure from a polaron to a bipolaron during the doping process.

As shown in Table 2, PEPPE and PEPMPE exhibit rare neutral green colors, while PBEPPE and PBEPMPBE display neutral gray colors. These results are in good agreement with the optical absorption spectra of the precursors, and the existence of the methyl group makes the maximum absorption peak of PEPMPE blueshift compared with that of PEPPE.

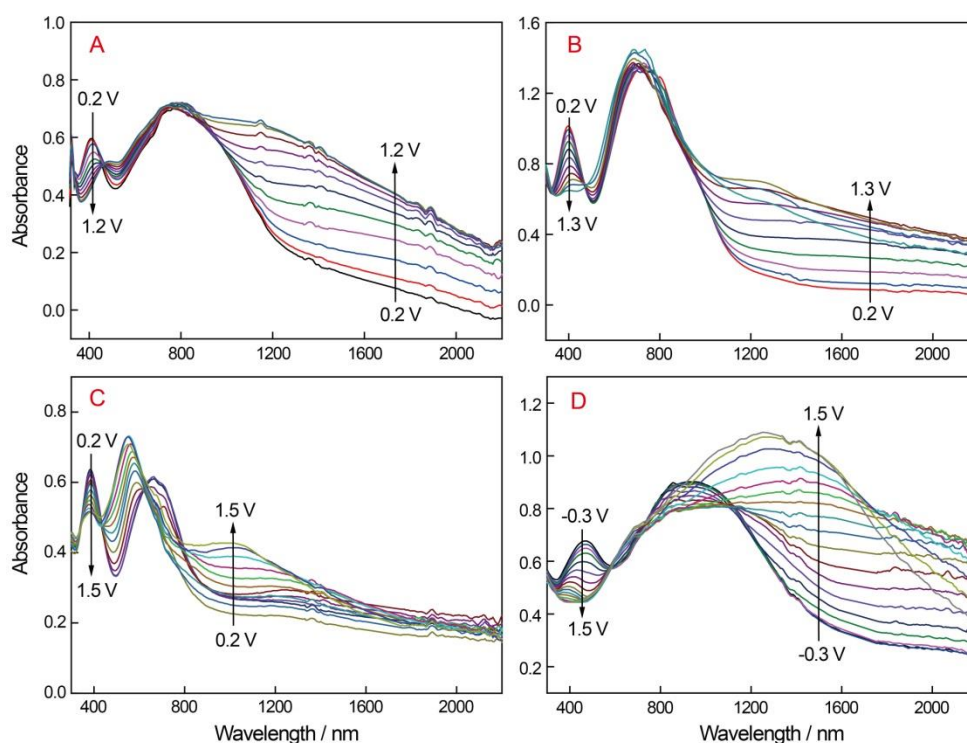


**Figure 6.** Spectroelectrochemistry of the PEPPE (A), PEPMPE (B), PBEPPE (C), PBEPMPBE (D) films in blank  $\text{CH}_2\text{Cl}_2\text{-Bu}_4\text{NPF}_6$  ( $0.10 \text{ mol L}^{-1}$ ).

Moreover, the stronger conjugation degree and electron-donating ability of BisEDOT are beneficial for reducing the LUMO energy level of the molecule, [7] which facilitates the redshift of the absorption peak of PBEPMPBE compared with that of PBEPPE and the color conversion from

neutral green for PEPMPE to neutral gray for PBEPMPBE. Additionally, the optical bandgaps ( $E_{g,opt}$ ) of the polymers are calculated as 1.01, 1.08, 1.42, and 0.82 for PEPPE, PEPMPE, PBEPPBE, and PBEPMPBE, respectively, which are lower than most reported green color polymers. [7, 37] Notably, the optical bandgap of PBEPMPBE decreases significantly by increasing the length of the conjugate chain, and this low bandgap contributes to decreasing the energy dissipation of the polymer in practical applications.

### 3.7.2 Kinetic studies

To measure the transmittance, response time, and coloring efficiency of different materials, the variation in transmittance in the visible and near-infrared regions of each polymer film are shown in Fig. 7, and the typical electrochromic parameters are summarized in Table 3. Specifically, the optical contrasts of PEPPE, PEPMPE, PBEPPBE, and PBEPMPBE were measured in the blank  $\text{CH}_2\text{Cl}_2\text{-Bu}_4\text{NPF}_6$  ( $0.1 \text{ mol L}^{-1}$ ) solution by optical spectroscopy coupled with a square-wave potential step method. The response time was calculated as the time required when the polymer achieved 95% of its maximum optical contrast to evaluate the time required for color conversion. The coloring efficiency was also calculated as the key factor to evaluate the energy utilization of these electrochromic materials.

The optical contrast of the four polymers in the visual region is inferior to that of other reported D-A-D type polymers [2, 37, 38] whereas the optical contrast in NIR region of the polymers with methyl-substituted acceptors, such as PEPMPE (60%) and PBEPMEBE (60%), is significantly higher than that of PEPPE (33%) or PBEPPBE (20%), and comparable to our previous works. [7] In addition, the four obtained polymers exhibit fast response times from 0.6 s to 3 s, especially PBEPMEBE, which achieves 95% of its optical contrast in only 0.80 s during the oxidation process and 0.60 s during the reduction process at 1500 nm. A short response time means that the polymer is more suitable for electrochromic devices because the short response time is conducive to a rapid change in material color. Moreover, the coloration efficiency of the four polymers is also satisfactory, and PEPMPE and PBEPMPBE reveal relatively high CE values of 324.32 and 234.82  $\text{cm}^2 \text{C}^{-1}$  at 1500 nm, respectively, implying that they are excellent electrochromic materials for use in near-infrared applications.

Open-circuit memory is another important parameter to evaluate electrochromic materials in practical applications. It refers to the ability of the polymer to maintain its color in an oxidation or reduction state at the open-circuit voltage. [2] The images of each polymer (Fig. 8) were also recorded in the visible and near-infrared regions with the application of square-wave voltages for 2 s and then turned off for 100 s as a complete cycle. After comparison, it can be concluded that the stability in the transmittance of the four polymers is better in the near-infrared region than in the visual region (excluding PEPPE), and the transmittance of PEPPE, PEPMPE, and PBEPMPBE are almost constant in the dedoping state.

**Table 2.** Electrochromic parameters of the green color polymers at different wavelengths

Polymers	Wavelength (nm)	$T_{\text{red}}$ (%)	$T_{\text{ox}}$ (%)	$\Delta T$ (%)	Response time (s)		Coloration efficiency ( $\text{cm}^2/\text{C}$ )
					Oxidation	Reduction	
PEPPE	400	50	66	16	1.20	1.20	67.22
	1350	90	57	33	1.20	1.90	152.15
PEPMPE	400	40	69	29	0.95	2.50	129.91
	1500	93	33	60	0.80	2.70	324.32
PBEPPBE	380	50	61	11	1.60	1.60	121.11
	1000	89	69	20	2.60	1.80	153.50
PBEPMPBE	460	40	56	16	2.80	1.60	130.70
	1500	95	35	60	0.80	0.60	234.82
PBOTT-BTD <sup>[37]</sup>	423	-	-	35	-	-	370
	650	-	-	23	-	-	303
PIDOHE <sup>[7]</sup>	424	35	65	30	0.98	0.68	64
	1500	78	19	59	0.75	1.34	105
PIDODE <sup>[7]</sup>	427	50	64	14	0.77	0.63	268
	1500	91	41	50	0.91	1.44	144

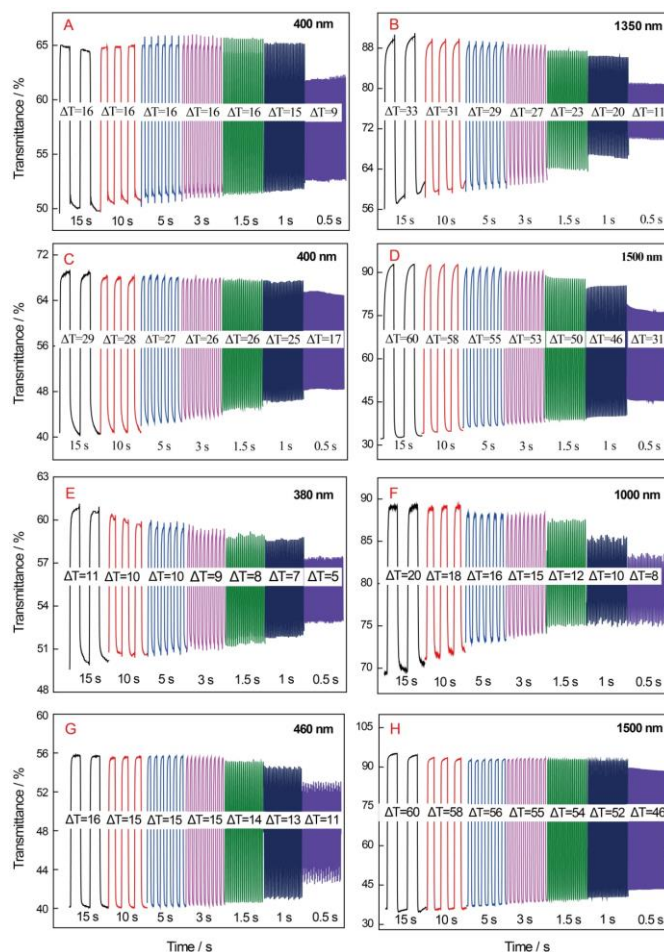


**Figure 7** Time-transmittance profiles of the PEPPE films at 400 nm (A) and 1350 nm (B), the PEPMPE films at 400 nm (C) and 1500 nm (D), the PBEPPBE films at 380 nm (E) and 1000 nm (F), and the PBEPMPBE films at 460 nm (G) and 1500 nm (H) at square-wave voltages from 0.2 V to 1.2 V, 0.2 V to 1.3 V, 0.2 V to 1.5 V, and -0.3 V to 1.5 V, respectively, for different switching time intervals (15 s-0.5 s).

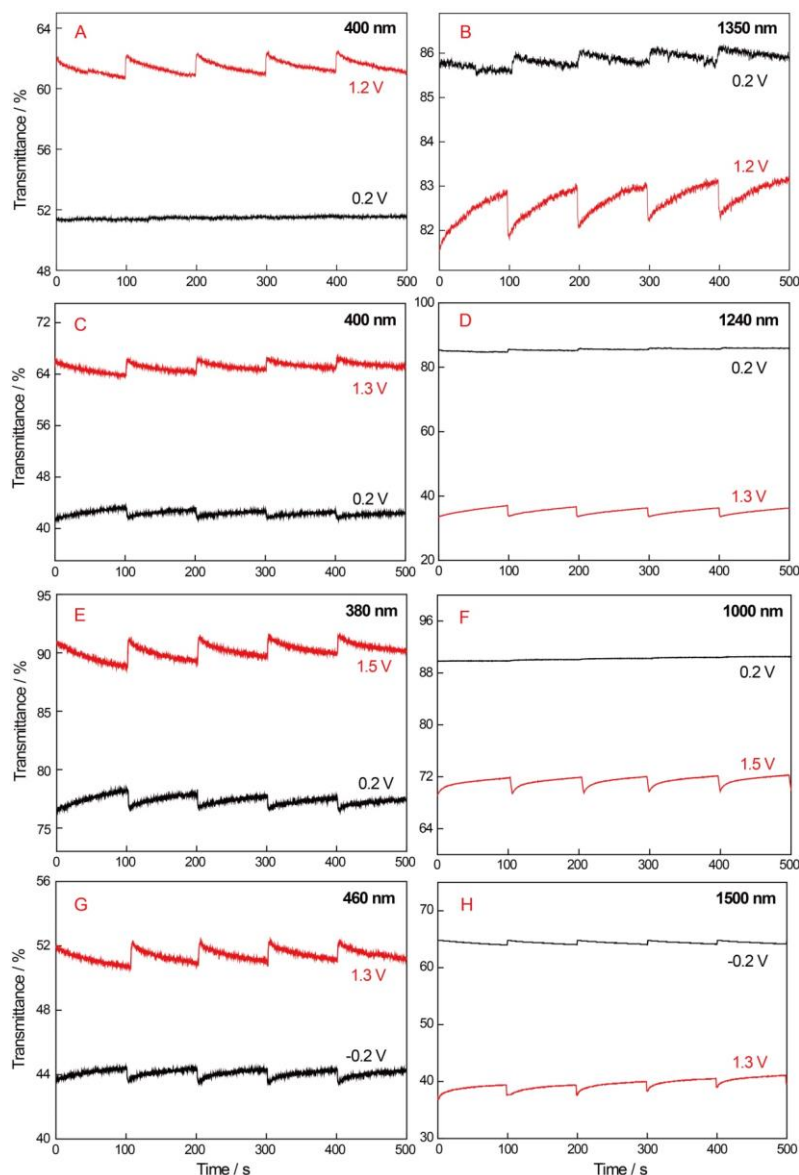


**Figure 8** Open-circuit memory of the PEPPE films at 400 nm (A) and 1350 nm (B), the PEPMPPE films at 400 nm (C) and 1240 nm (D), the PBEPPE films at 380 nm (E) and 1000 nm (F), and the PBEPMPPE films at 460 nm (G) and 1500 nm (H).

The weak change in transmittance in the near-infrared region means that the ability of the materials to maintain their color under open-circuit conditions is better, which reveals that a small consumption of energy can maintain the color state of the material in practical applications.

#### 4. CONCLUSION

In this work, four precursors were synthesized using *Stille* coupling and electropolymerized to form conducting hybrid polymers with excellent near-infrared electrochromic properties. The structure-property relationships of the precursors and hybrid polymers, including their optoelectronic,

electrochemical, and electrochromic properties, and even their quantum chemistry calculations and morphologies, were systematically explored.

Cyclic voltammetry shows low oxidation potentials ranging from 0.88 to 0.82 V for EPPE to EPMPE and 0.72 to 0.71 V for BEPPBE to BEPMPBE, which implied that the molecules modified by methyl groups had better solubility; thus, these materials could be easily electrodeposited as uniform hybrid polymer films at low oxidation potentials. In regard to the hybrid polymers, PEPPE and PEPMPBE exhibited neutral green colors, while PBEPPE and PBEPMPBE displayed neutral gray colors after combining with the stronger donor. Moreover, the conjugated chain lengths of PBEPPE and PBEPMPBE were extended by introducing BisEDOT, which accounted for the redshift in their absorption spectra, along with their low optical bandgap, fast response time, high optical contrast, and coloration efficiency in the near-infrared region. The hybrid polymers showed planar  $\pi$ -conjugated backbones with relatively compact particle and rod-like morphologies; in particular, the PBEPMPBE films showed a porous structure that was beneficial for providing the highest optical contrast (60%) and lowest response time (0.6 s). These four materials broaden the range of electrochromic neutral green and gray polymers and show promise for use in display applications.

#### SUPPLEMENTARY MATERIAL:

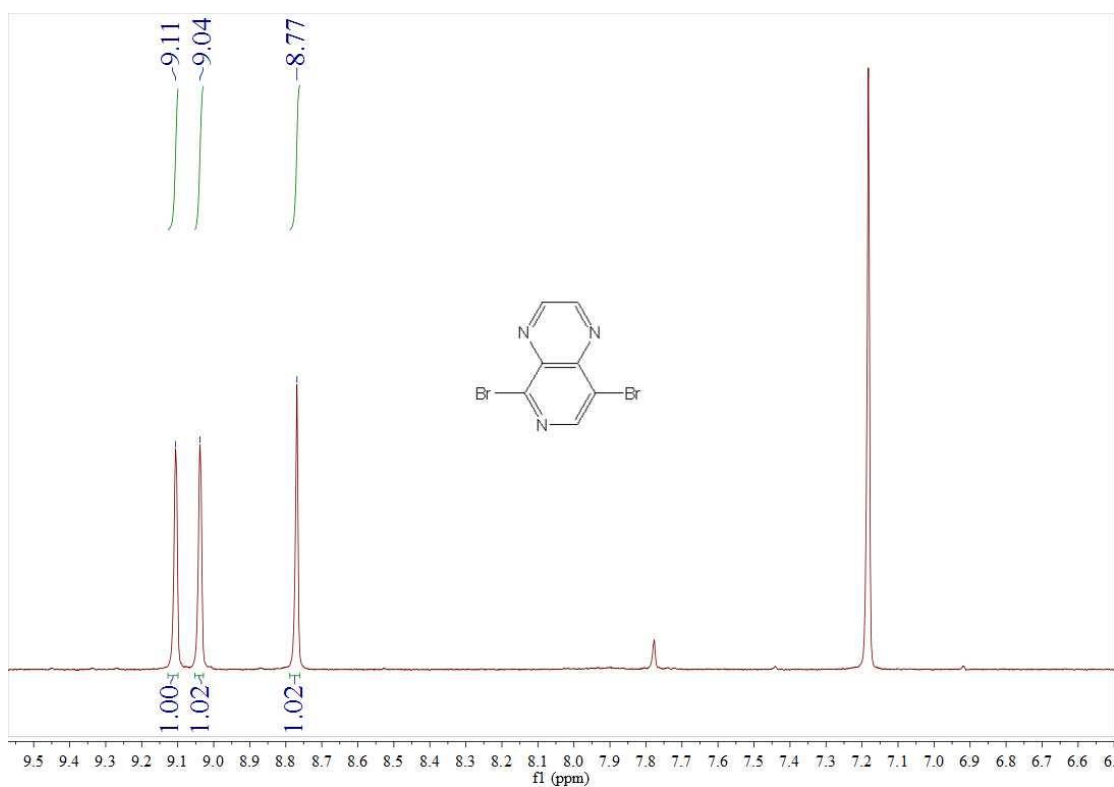


**Figure S1.** <sup>1</sup>H NMR spectrum of Br-PP-Br dissolved in CDCl<sub>3</sub>.

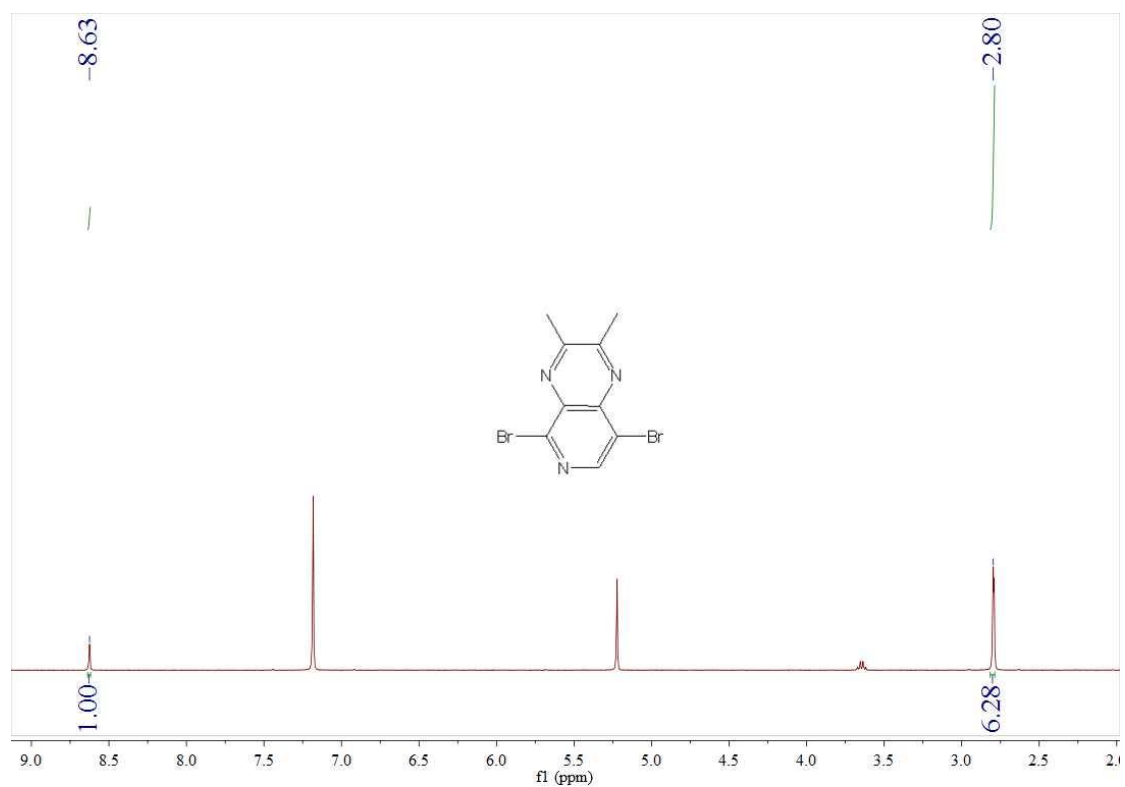


**Figure S2.** <sup>1</sup>H NMR spectrum of Br-PMP-Br dissolved in CDCl<sub>3</sub>.

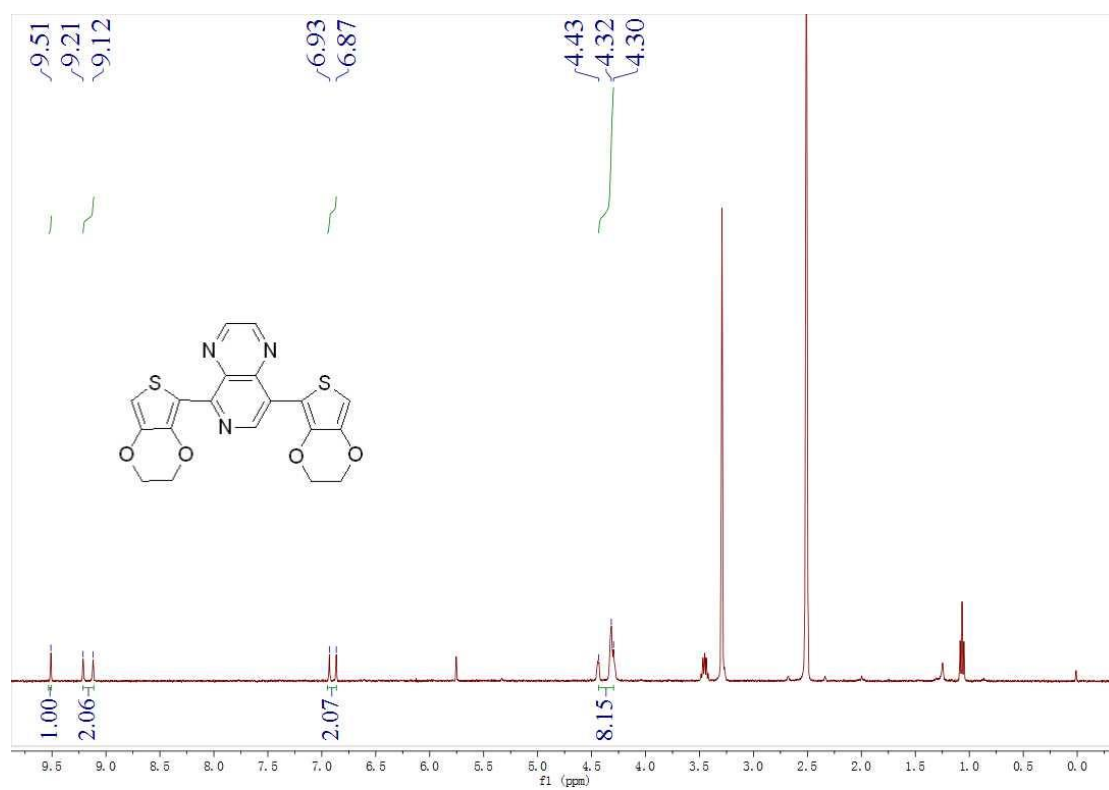


**Figure S3.** <sup>1</sup>H NMR spectrum of EPPE dissolved in DMSO-*d*<sub>6</sub>.

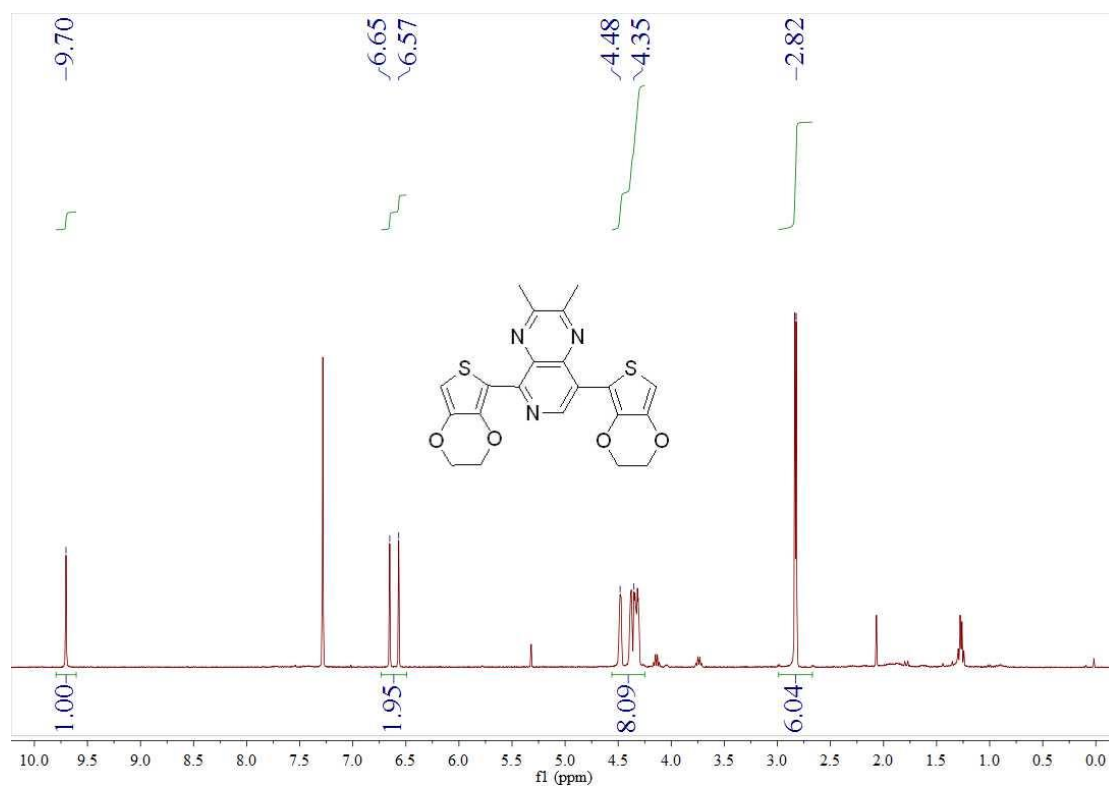


Figure S4. <sup>1</sup>H NMR spectrum of EPMPE dissolved in CDCl<sub>3</sub>.

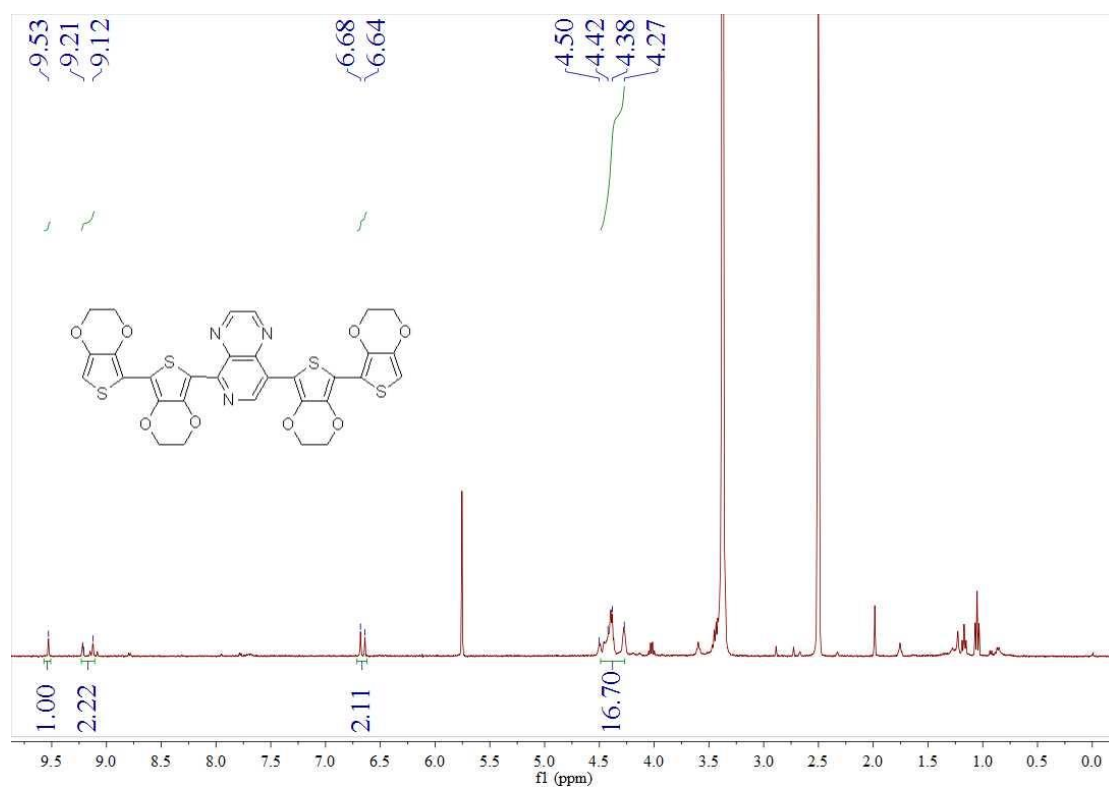
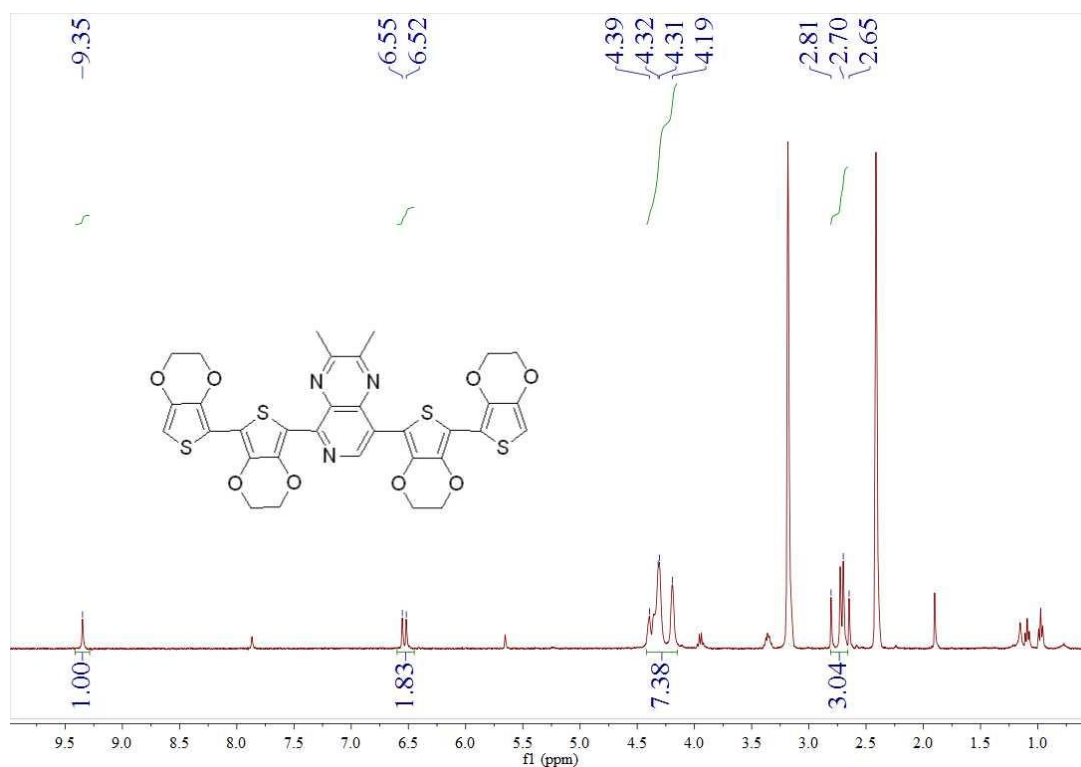
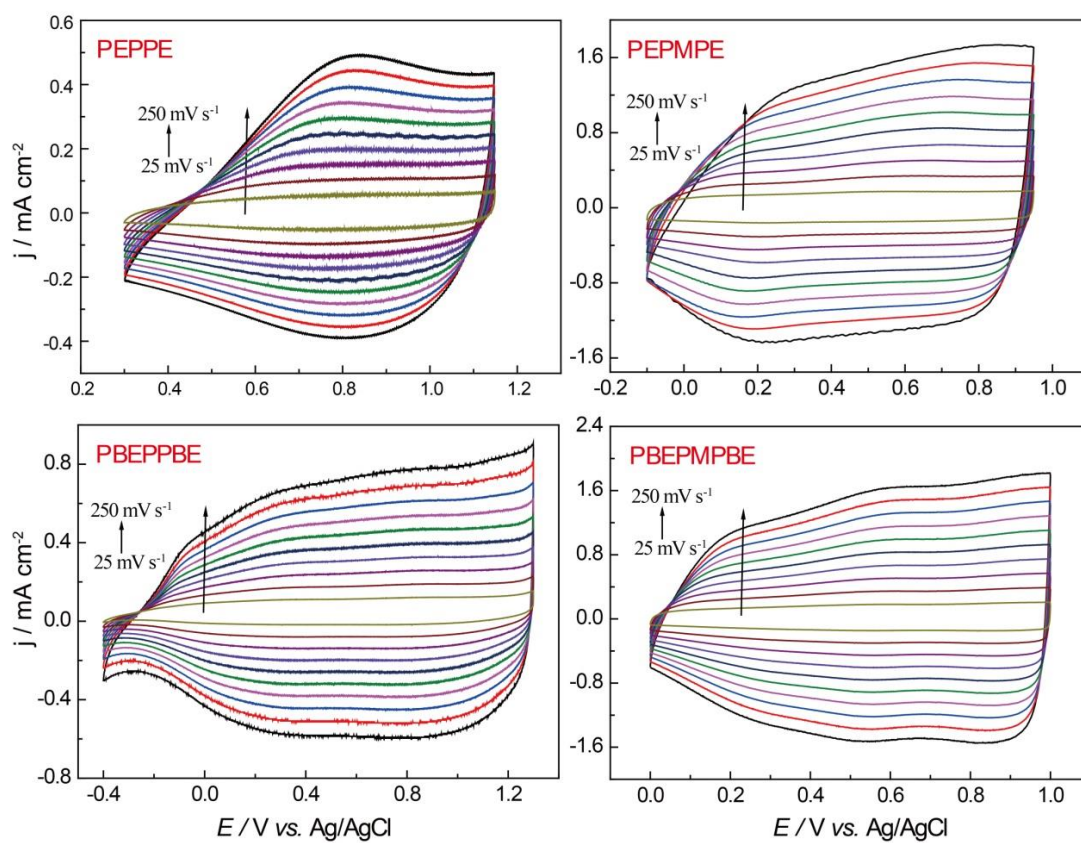


Figure S5. <sup>1</sup>H NMR spectrum of BEPPBE dissolved in DMSO-*d*<sub>6</sub>.



**Figure S6.**  $^1\text{H}$  NMR spectrum of BEPMPBE dissolved in  $\text{DMSO-}d_6$ .

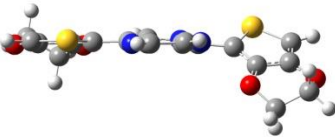
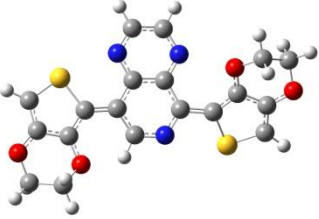
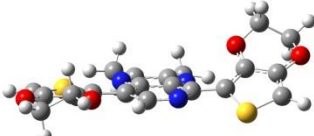
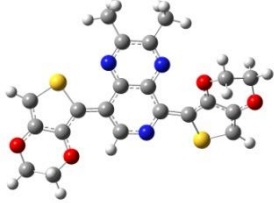
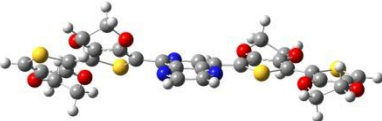
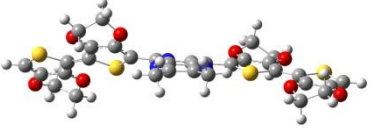
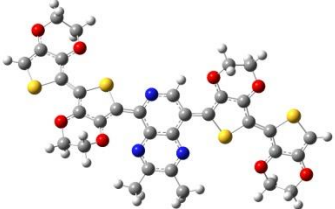


**Figure S7.** CVs of the PEPPE, PEPMPE, PBEPPE, and PBEPMPBE films in blank  $\text{MeCN-Bu}_4\text{NPF}_6$  (0.1 M) at potential scan rates of 250, 200, 150, 100, 50, 25  $\text{mV s}^{-1}$ .

**Table S1.** Infrared absorption peak assignment for the precursors and polymers

Peaks (cm <sup>-1</sup> )		Assignment
EPPE/EPMPPE	PEPPE/PEPMPE	
3101, 2964, 2919/3101, 2925, 2871	—	=C–H vibration of thiophene
1652/1570	1586/1590	ring vibration of substituted pyridine
1470, 1372/1445, 1361	1438, 1358/1433, 1355	ring vibration of substituted thiophene
1207~1048/1064	—	=C–H in-plane of thiophene
801/911, 845	—	=C–H out-of-plane of thiophene
—	840	PF <sub>6</sub> <sup>-</sup>
Peaks (cm <sup>-1</sup> )		Assignment
BEPPBE/BEPMPBE	PBEPPBE/PBEPMPBE	
2979, 2926, 2871/2949, 2919, 2871	—	=C–H vibration of thiophene
1504, 1457/1493, 1451	1439, 1361/1397, 1355	ring vibration of substituted pyridine
1361/1361	1217/1217	ring vibration of substituted thiophene
1061/1067	—	=C–H in-plane of thiophene
905/899	—	=C–H out-of-plane of thiophene
—	840	PF <sub>6</sub> <sup>-</sup>

**Table S2.** Optimized geometries of the precursors in different views

Precursors	Side view	Top view
EPPE		
EPMPE		
BEPPBE		
BEPMPBE		

#### ACKNOWLEDGEMENTS

This work was supported by the National Natural Science Foundation of China (grant numbers 51763010 and 51963011), the Technological Expertise and Academic Leaders Training Program of Jiangxi Province (grant number 20194BCJ22013), the Educational Science Planning Project of Jiangxi Province (19YB137), the Science and Technology Project of the Education Department of Jiangxi Province (GJJ190622), and the Research Project of the State Key Laboratory of Mechanical System and Vibration (grant number MSV202013).

#### References

1. C. I. F, in *Nonemissive Electrooptic Displays*, Springer US (1976).
2. R. B. J. R, *Chemical Reviews*, 110 (2010) 268.
3. S. C. Yu Xue, Jiarui Yu, Benjamin R. Bunes, Zexu Xue, Jingkun Xu, Baoyang Lu and Ling Zang, *Journal of Materials Chemistry C*, 8 (2020) 10136.
4. S. Ming, S. Zhen, X. Liu, K. Lin, H. Liu, Y. Zhao, B. Lu and J. Xu, *Polymer Chemistry*, 6 (2015) 8248.
5. F. Hu, W. Zhang, Y. Xue, K. Lin, B. Lu, J. Xu and G. Zhao, *Materials Chemistry and Physics*, 244 (2020) 122699.
6. Y. Xue, Z. Xue, W. Zhang, W. Zhang, S. Chen, K. Lin and J. Xu, *Journal of Electroanalytical Chemistry*, 834 (2019) 150.
7. H. Gu, S. Ming, K. Lin, S. Chen, X. Liu, B. Lu and J. Xu, *Electrochimica Acta*, 260 (2018) 772.

8. N. Jian, H. Gu, S. Zhang, H. Liu, K. Qu, S. Chen, X. Liu, Y. He, G. Niu, S. Tai, J. Wang, B. Lu, J. Xu and Y. Yu, *Electrochimica Acta*, 266 (2018) 263.
9. K. Lin, S. Chen, B. Lu and J. Xu, *Science China Chemistry*, 60 (2016) 38.
10. B. Lu, S. Ming, K. Lin, S. Zhen, H. Liu, H. Gu, S. Chen, Y. Li, Z. Zhu and J. Xu, *New Journal of Chemistry*, 40 (2016) 8316.
11. F. Hu, Y. Xue, N. Jian, K. Qu, K. Lin, X. Zhu, T. Wu, X. Liu, J. Xu and B. Lu, *Electrochimica Acta*, 357 (2020) 136859.
12. G. E. Gunbas, A. Durmus and L. Toppare, *Advanced Materials*, 20 (2008) 691.
13. H. Zhao, Y. Wei, J. Zhao and M. Wang, *Electrochimica Acta*, 146 (2014) 231.
14. M. Nikolou, A. L. Dyer, T. T. Steckler, E. P. Donoghue, Z. Wu, N. C. Heston, A. G. Rinzler, D. B. Tanner and J. R. Reynolds, *Chemistry of Materials*, 21 (2009) 5539.
15. A. K. A. Dubois C J , Reynolds J R., *Journal of Physical Chemistry B*, 108 (2004) 8550.
16. G. G. Durmus A, Toppare L, et al., *Chemistry of Materials*, 19 (2007) 6247.
17. G. Sonmez, Schwendeman I, Schottland P , et al., *Macromolecules*, 36 (2003) 639.
18. G. E. Gunbas, A. Durmus and L. Toppare, *Advanced Functional Materials*, 18 (2008) 2026.
19. B. Lu, S. Zhen, S. Zhang, J. Xu and G. Zhao, *Polymer Chemistry*, 5 (2014) 4896.
20. H. Shi, C. Liu, Q. Jiang and J. Xu, *Advanced Electronic Materials*, 1 (2015) 1500017.
21. J. R. R. Gregory A. Sotzing, Peter J. Steel, *Chemistry of Materials*, 8 (1996) 882.
22. C. G. Granqvist, E. Avendaño and A. Azens, *Thin Solid Films*, 442 (2003) 201.
23. R. J. Akoudad S *Synthetic Metals*, 93 (1998) 0.
24. S. Ming, S. Zhen, X. Liu, K. Lin, H. Liu, Y. Zhao, B. Lu and J. Xu, *Polymer Chemistry*, 6 (2015) 8248.
25. H. Gu, Y. Xue, F. Hu, N. Jian, K. Lin, T. Wu, X. Liu, J. Xu and B. Lu, *Dyes and Pigments*, 183 (2020) 108648.
26. G. L. Gibson, T. M. McCormick and D. S. Seferos, *Journal of the American Chemical Society*, 134 (2012) 539.
27. M. İçli-Özkut, H. İpek, B. Karabay, A. Cihaner and A. M. Önal, *Polymer Chemistry*, 4 (2013) 2457.
28. L. B. Zhen S , Xu J , et al., *RSC Advances*, 4 (2014) 14001.
29. M. S. Lin K, Zhen S, et al., *Polymer Chemistry*, 6 (2015) 4575.
30. M. D. Feng Z , Wang Z , et al, *Electrochimica Acta*, 160 (2015) 160.
31. L. Baoyang, K. Lin, S. Zhen, S. Ming, H. Liu, H. Gu, S. Chen and J. Xu, *Synthetic Metals*, 220 (2016) 202.
32. K. Lin, Y. Zhao, S. Ming, H. Liu, S. Zhen, J. Xu and B. Lu, *Journal of Polymer Science Part A: Polymer Chemistry*, 54 (2016) 1468.
33. S. Nad and S. Malik, *ChemElectroChem*, 7 (2020) 4144.
34. S. Ming, S. Zhen, K. Lin, L. Zhao, J. Xu and B. Lu, *ACS applied materials & interfaces*, 7 (2015) 11089.
35. B. Lu, Y. Li and J. Xu, *Journal of Electroanalytical Chemistry*, 643 (2010) 67.
36. J. Nannan, Kai, et al., *Physical chemistry chemical physics* 21 (2019) 7174.
37. W. Li, Y. Guo, J. Shi, H. Yu and H. Meng, *Macromolecules*, 49 (2016) 7211.
38. S. Al-Ogaidi, B. Karabay, L. C. Karabay and A. Cihaner, *Journal of Electroanalytical Chemistry*, 768 (2016) 1.